



HAL
open science

Maxwell stress-induced flow control of a free surface electro-osmotic flow in a rectangular microchannel

Manik Mayur, Sakir Amiroudine, Didier Lasseux, Suman Chakraborty

► **To cite this version:**

Manik Mayur, Sakir Amiroudine, Didier Lasseux, Suman Chakraborty. Maxwell stress-induced flow control of a free surface electro-osmotic flow in a rectangular microchannel. *Microfluidics and Nanofluidics*, 2014, 16 (4), pp.721-728. 10.1007/s10404-013-1262-1 . hal-03830448

HAL Id: hal-03830448

<https://hal.science/hal-03830448v1>

Submitted on 2 Dec 2022

HAL is a multi-disciplinary open access archive for the deposit and dissemination of scientific research documents, whether they are published or not. The documents may come from teaching and research institutions in France or abroad, or from public or private research centers.

L'archive ouverte pluridisciplinaire **HAL**, est destinée au dépôt et à la diffusion de documents scientifiques de niveau recherche, publiés ou non, émanant des établissements d'enseignement et de recherche français ou étrangers, des laboratoires publics ou privés.



Distributed under a Creative Commons Attribution 4.0 International License

Maxwell stress-induced flow control of a free surface electro-osmotic flow in a rectangular microchannel

Manik Mayur · Sakir Amiroudine ·
Didier Lasseux · Suman Chakraborty

Abstract Multiphase flow control is a challenging task in microfluidic systems. Application of such ideas in electro-osmotic actuation of multiphase flows, which involves a complex convolution of phenomena ranging from electro-chemistry to hydrodynamics, is even more tricky. Most of the existing studies in the field have limited their scope to the thin electric double layer (EDL) limit, where the role of ionic space charge distribution in the EDL is simplified to provide a slip velocity boundary condition at the substrate, and the role of the fluid–fluid interface is limited to continuity of velocity and hydrodynamic shear stress. In this study, electro-osmotic flow of two immiscible fluids, an electrolytic solution and an inert gas, are studied in a rectangular microchannel and the role of interfacial potential and Maxwell stress-generated dynamics is explored in a wide range of EDL thicknesses. A net stress term is used in the transport equations which includes the electric effects by Maxwell stress as well as the hydrodynamic stress. It is observed that the free surface, depending upon its potential may enhance the fluid velocity or act as a rigid wall. With the help of two-dimensional velocity contour plots, the role of various flow parameters on flow profile is discussed. Further, a parametric analysis of flow rate gives interesting insights into the flow rate reversal and control in such microfluidic devices.

Keywords Electro-osmosis · Rectangular cavity · Free surface · Maxwell stress

1 Introduction

Electro-osmotic flows have a characteristic advantage over classical pressure-driven flows such as, uniform and non-dispersive velocity profile, easier flow control, no physical moving parts etc. However, the flow rates achieved in microdevices are limited by the device geometry through micro-fabrication constraints and magnitude of the actuating field. In addition, electro-osmotic transport induces flow rate fluctuations due to localized changes in the ionic concentrations and pH. To have a better control over such a flow, one must have a better understanding of convoluted dependence of flow parameters on the fluid, substrate and the electric field interactions. Over the past few years, rigorous studies have attempted to delineate the detailed physics of single and multiphase systems which include various ranges of ionic concentration, dielectric properties along with constant and modulated electric fields (Ramos 2011; Chang et al. 2012; Lin 2009). Most of the previous studies have limited their scope to thin EDL where the role of space charge distribution in EDL is limited to provide a slip velocity in the bulk dynamics. However, when the extent of such a space charge distribution is significant as compared to the characteristic length scales, there is a significant alteration in the velocity distribution (Bhattacharyya et al. 2005). Also, the behavior of such a system when it encounters a material discontinuity in the form of a charge storing interface is still under-explored. Specially, the behavior of air–liquid interface and the associated surface charge is not clearly understood and various models explaining the same are available in the literature (Levin et al. 2009). The

M. Mayur · S. Amiroudine · D. Lasseux
Université Bordeaux 1, I2M-TREFLE, UMR CNRS 5295,
16 Av. Pey-Berland, 33607 Pessac, France

S. Chakraborty
Department of Mechanical Engineering, Indian Institute of
Technology, Kharagpur 721302, India

existence of air–liquid interfacial flows in confined micro-scale geometries is commonly observed in a wide range of applied systems such as liquid–gas displacement in porous structures (Churaev 2000), microstructure controlled wettability (Lotus effect) (Marmur 2004), controlled biological cell growth systems (Bose et al. 2012), air bubbles trapped in micro-capillaries (Schoch et al. 2008) etc. The recent study of two-phase electro-osmotic systems such as air–water systems has highlighted the role of interfacial charges on the velocity profile (Gao et al. 2005a, b) such as different interfacial and bulk velocities, a feature that is unexpected in a classical EOF. Such a highly dispersive velocity profile can affect the species transport (Griffiths and Nilson 2006) using EOF. In addition to electro-chemical properties of the system, which determine the liquid–gas and liquid–solid interfacial zeta potentials and charge distribution, the role of confining walls on the velocity distribution cannot be ignored. The common approach of two-dimensional EOF models predicts the velocity profiles by ignoring the confinement effects which are useful when channel aspect ratios are significantly larger than the EDL thickness. However, due to various micro-fabrication limitations and practical aspects of microfluidic devices, large aspect ratio micro-channels are not very common. This requires a three-dimensional analysis of the flow to understand the flow profiles especially when the channel dimensions are comparable to the EDL thickness. In the present study, electro-osmotic flow of two immiscible fluids with a flat interface is studied in a rectangular microchannel and the role of interfacial potential and Maxwell stress-generated dynamics is explored. Such a system represents basic state of a generalized stability analysis problem which is important for flow control and mixing in microdevices. The two-fluid system consists of an inert gas that, due to viscosity and permittivity contrasts with underlying liquid, is considered to remain at constant pressure and an electrolytic solution which is actuated electro-osmotically. Such a system highlights the role of interfacial Maxwell stress-generated dynamics on a free surface where the classical condition is limited to the continuity of shear stress. Such flows have also found many applications in microfluidic devices such as biological cell culture experiments (Bose et al. 2012). A net stress term is used in the equations which includes the electric effects by Maxwell stress as well as the hydrodynamic stress. This approach is different from the classical approach of using an electrical body force term in the momentum equations and facilitates the demonstration that stress jump condition on an interface is not limited to the classical condition on the net hydrodynamic shear stress for a flat interface (Lee and Li 2006; Choi et al. 2010; Mayur et al. 2012; Ozen et al. 2006). The interfacial potential can be attributed to the electro-chemistry of the interacting system. The electrostatic potential distribution is obtained by solving

the linearized Poisson–Boltzmann equation for low zeta potential systems while assuming that the external field does not affect the space charge distribution in the fluid. The fluid velocity is obtained from the Stokes equation while using the mentioned modified stress term. The flow rate variation for the system is studied for a wide range of parameters exhibiting interesting phenomena like flow rate enhancement and reversal in such systems.

2 Mathematical modelling

The system under consideration consists of two fluids having a planar interface in a microchannel with a rectangular cross section. A Cartesian coordinate system is chosen to describe the channel geometry where the origin is set at the intersection of the bottom wall and the transverse line of symmetry (see Fig. 1). The width of the channel is taken as $2l$. The height of the bottom fluid (Fluid 1) is taken as h_1 and the top fluid is taken as h_2 . The bottom fluid is considered to be a low-concentration symmetrical electrolytic solution with constant permittivity (ϵ_1). The top fluid (Fluid 2) is considered to be a low permittivity ($\epsilon_2 \sim 1$), low viscosity ($\mu_2 \sim 0$) and inert gas phase that remains hence unaffected by the flow and is kept at constant pressure. Henceforth, only the dynamics of Fluid 1 will be explored. Electrical double layers form at the interface between the electrolyte and the bounding walls as well as at the liquid–gas interface. All the interfaces with the electrolytic solution develop zeta potentials, the magnitude of which depends upon the electro-chemistry of liquid–gas and solid–liquid interactions. The bottom wall zeta potential is taken as ζ_b , the side wall zeta potential is

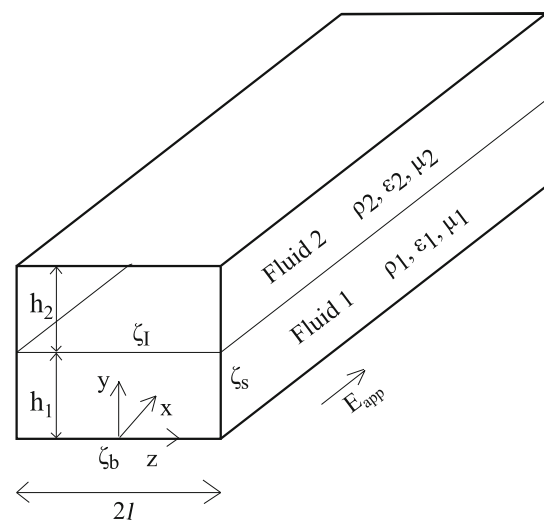


Fig. 1 Schematic representation of the system. Fluid 1 is an ionic solution with constant properties. Fluid 2 is a low permittivity, low viscosity inert gas at a constant pressure

taken as ζ_s , and the liquid–gas interfacial zeta potential is taken as ζ_l . It is assumed that the external electric field has no effect on the substrate and interfacial zeta potentials. The bounding walls are considered to be rigid and a constant electric field is applied along the channel length (x -direction). Due to the symmetry of the system along $z = 0$, the governing equations will be solved for $0 \leq z \leq l$ and $0 \leq y \leq h_1$.

2.1 Electrostatic potential distribution

The electrostatic potential distribution in Fluid 1 due to the space charge distribution ($\phi_{1,sc}$) can be expressed by Gauss law as,

$$-\vec{\nabla} \cdot (\epsilon_1 \vec{\nabla} \phi_{1,sc}) = \rho_e = \sum_i e z_i C_i \tag{1}$$

where ρ_e is the net charge density, e is the electronic charge, z_i is the valence of the ions, C_i is the ionic concentration of the i th ionic species and ϵ_1 is the permittivity of fluid 1. The charge transport equation in fluid 1 can be modeled using the Poisson–Nernst–Planck equation as,

$$\frac{\partial C_i}{\partial t} + \vec{\nabla} \cdot (\vec{u}_1 C_i) = \vec{\nabla} \cdot (D_i \vec{\nabla} C_i) + \frac{z_i e}{k_B \theta} \vec{\nabla} \cdot (D_i C_i \vec{\nabla} \phi_{1,sc}) \tag{2}$$

where \vec{u}_1 is the convective velocity field of fluid 1, D_i is the diffusivity of the i th ionic species, k_B is the Boltzmann constant and θ is the liquid temperature. In constricted geometries having the characteristic length scales of the order of micro and nanometers along with a weaker advective transport in a viscosity dominated regime, the ionic Peclet number is low regardless of small ionic diffusivity ($D_i \sim 10^{-9}$ m²/s). In such cases, the advective transport of ionic species can be neglected as compared to the diffusive transport. Along with a steady flow assumption, the resulting quasi-equilibrium system gives from Eq. (2) a Boltzmann distribution of ionic species in the solution as,

$$C_i = C_{0,i} \exp\left(-\frac{z_i e \phi_{1,sc}}{k_B \theta}\right) \tag{3}$$

where $C_{0,i}$ is the bulk concentration of i th ionic species. Considering the electrolyte to be symmetrical ($|z_+| = |z_-| = z_0$) with constant permittivity, one can obtain the classical Poisson–Boltzmann equation (PBE) from Eqs. (1) and (3) as,

$$\epsilon_1 \nabla^2 \phi_{1,sc} = 2z_0 e C_0 \text{Sinh}\left(\frac{z_0 e \phi_{1,sc}}{k_B \theta}\right) \tag{4}$$

Upon using the scaling parameters as, $X = x/D_h, Y = y/D_h, Z = z/D_h, \Phi_{1,sc} = \phi_{1,sc}/\zeta_b$, where $D_h = 4lh_1/(l+h_1)$ is the hydraulic diameter of an open rectangular duct, and using Debye–Huckel linearization for small wall potentials (~ 25 mV), the governing equation for the electrostatic potential distribution in the EDL can be obtained as,

$$\frac{\partial^2 \Phi_{1,sc}}{\partial Y^2} + \frac{\partial^2 \Phi_{1,sc}}{\partial Z^2} = \frac{\Phi_{1,sc}}{De^2} \tag{5}$$

where, $De = \lambda_D/D_h$ is the Debye number which represents the relative extent of the EDL as compared to the geometric length scale with $\lambda_D = \sqrt{\epsilon k_B \theta / (2\rho_0 z^2 e^2)}$. The electrostatic potential distribution satisfies the following boundary conditions,

$$\begin{aligned} \frac{\partial \Phi_{1,sc}}{\partial Z}(Y, 0) &= 0, & \Phi_{1,sc}(Y, L) &= \bar{\zeta}_s, \\ \Phi_{1,sc}(0, Z) &= \bar{\zeta}_b, & \Phi_{1,sc}(H_1, Z) &= \bar{\zeta}_l \end{aligned} \tag{6}$$

where $L = l/D_h, H_1 = h_1/D_h, \bar{\zeta}_s = \zeta_s/\zeta_b, \bar{\zeta}_b = 1$ and $\bar{\zeta}_l = \zeta_l/\zeta_b$. The solution of Eqs. (5) and (6) can be obtained by separation of variables as,

$$\begin{aligned} \Phi_{1,sc}(Y, Z) = & \sum_{m=1}^{\infty} \frac{2(-1)^{m-1} \left[\bar{\zeta}_l \text{Sinh}\left(\sqrt{1/De^2 + \lambda_m^2} Y\right) + \bar{\zeta}_b \text{Sinh}\left(\sqrt{1/De^2 + \lambda_m^2} (H_1 - Y)\right) \right] \text{Cos}(\lambda_m Z)}{L \lambda_m \text{Sinh}\left(\sqrt{1/De^2 + \lambda_m^2} H_1\right)} \\ & + \sum_{n=1}^{\infty} \frac{2(1+(-1)^{n-1}) \bar{\zeta}_s \text{Cosh}\left(\sqrt{1/De^2 + \lambda_n^2} Z\right) \text{Sin}(\lambda_n Y)}{H_1 \lambda_n \text{Sinh}\left(\sqrt{1/De^2 + \lambda_n^2} L\right)} \end{aligned} \tag{7}$$

where $\lambda_m = (2m - 1)\pi/(2L)$ and $\lambda_n = n\pi/H_1$. The electric potential due to the external field can be calculated as,

$$\Phi_{1,app}(X) = - \int \frac{E_{app} D_h}{\zeta_b} dX = - \frac{X}{E_R} \tag{8}$$

where $E_R = \zeta_b/E_{app} D_h$ is the ratio of the electric potential due to charge polarization in the electrolyte over the electric potential due to the externally applied electric field. Hence, the net electric potential field in the fluid 1 is

$$\Phi_1(X, Y, Z) = \Phi_{1,app}(X) + \Phi_{1,sc}(Y, Z) \tag{9}$$

2.2 Velocity distribution

Since fluid 2 is considered to be a low permittivity, low viscosity inert gas at a constant pressure, it can be considered at rest, i.e. $\vec{u}_2 = \vec{0}$. The external electric field along with the presence of space charge distribution in fluid 1 generates a Maxwell stress distribution in the fluid, which in the absence of magnetic field can be expressed as,

$$\vec{\Sigma}^M = - \frac{\epsilon_1 |\vec{E}|^2}{2} \vec{I} + \epsilon_1 \vec{E} \otimes \vec{E} \tag{10}$$

The Maxwell stress along with the hydrodynamic stress results into a net stress distribution in the fluid which can be expressed as,

$$\begin{aligned} \overleftrightarrow{\Sigma}^T &= \overleftrightarrow{\Sigma}^H + \overleftrightarrow{\Sigma}^M \\ &= - \left(p_1 + \frac{\varepsilon_1 |\vec{E}|^2}{2} \right) \overleftrightarrow{I} + \mu_1 \left(\overleftrightarrow{\nabla} \vec{u}_1 + \overleftrightarrow{\nabla} \vec{u}_1^T \right) + \varepsilon_1 \vec{E} \otimes \vec{E} \end{aligned} \quad (11)$$

where, $\overleftrightarrow{\Sigma}^T$ is the total stress tensor, p_1 is the hydrostatic pressure field in the liquid, μ_1 is the dynamic viscosity, \overleftrightarrow{I} is the unit tensor and $\vec{E} = -\overleftrightarrow{\nabla} \phi_1$ is the total electric field in the fluid. For a Newtonian fluid under incompressible flow, the conservation of mass and momentum equations can be written, respectively, as,

$$\overleftrightarrow{\nabla} \cdot \vec{u}_1 = 0 \quad (12a)$$

$$\begin{aligned} \rho_1 \left(\frac{\partial \vec{u}_1}{\partial t} + \left(\vec{u}_1 \cdot \overleftrightarrow{\nabla} \right) \vec{u}_1 \right) &= \overleftrightarrow{\nabla} \cdot \overleftrightarrow{\Sigma}^T \\ &= -\overleftrightarrow{\nabla} p_1 + \mu_1 \nabla^2 \vec{u}_1 + \overleftrightarrow{\nabla} \cdot \overleftrightarrow{\Sigma}^M \end{aligned} \quad (12b)$$

At the liquid–gas interface ($y = h_1$)

$$[\vec{t} \cdot \Sigma^T \cdot \vec{n}] = 0, \quad [\vec{n} \cdot \Sigma^T \cdot \vec{n}] = 0 \quad (13b)$$

At the symmetry plane ($z = 0$):

$$\frac{\partial \vec{u}_1}{\partial z} = \vec{0} \quad (13c)$$

The flow is considered to be laminar ($\vec{u}_1 = (u_1, 0, 0)$), steady and fully developed ($u_1 = u_1(y, z)$) and no external pressure gradient is applied. Upon rescaling the velocity as $U_1 = u_1/U_{\text{ref}}$, the governing equation reduces to,

$$\frac{\partial^2 U_1}{\partial Y^2} + \frac{\partial^2 U_1}{\partial Z^2} = \gamma_R \left(\frac{\partial^2 \Phi_1}{\partial Y^2} + \frac{\partial^2 \Phi_1}{\partial Z^2} \right) \quad (14)$$

where, $\gamma_R = (\varepsilon_1 E_{\text{app}} \zeta_b) / (\mu_1 U_{\text{ref}})$ is the electro-viscous number. The corresponding dimensionless boundary conditions are,

$$\begin{aligned} U_1(0, Z) = 0, \quad \frac{\partial U_1}{\partial Y}(H_1, Z) &= \gamma_R \frac{\partial \Phi_1}{\partial Y}(H_1, Z), \\ U_1(Y, L) = 0, \quad \frac{\partial U_1}{\partial Z}(Y, 0) &= 0, \end{aligned} \quad (15)$$

The solution to the Eqs. (14) and (15) can be obtained by using separation of variables as,

$$\begin{aligned} U_1(Y, Z) &= \sum_{m=1}^{\infty} \frac{2(-1)^{m-1} \gamma_R \left[\bar{\zeta}_I \text{Sinh} \left(\sqrt{1/De^2 + \lambda_m^2} Y \right) + \bar{\zeta}_b \text{Sinh} \left(\sqrt{1/De^2 + \lambda_m^2} (H_1 - Y) \right) \right] \text{Cos}(\lambda_m Z)}{L \lambda_m \text{Sinh} \left(\sqrt{1/De^2 + \lambda_m^2} H_1 \right)} \\ &+ \sum_{n=1}^{\infty} \frac{2 \left(1 + (-1)^{n-1} \right) \gamma_R \bar{\zeta}_s \text{Cosh} \left(\sqrt{1/De^2 + \lambda_n^2} Z \right) \text{Sin}(\lambda_n Y)}{H_1 \lambda_n \text{Cosh} \left(\sqrt{1/De^2 + \lambda_n^2} L \right)} \\ &+ \sum_{m=1}^{\infty} \frac{2(-1)^m \gamma_R \bar{\zeta}_b \text{Cosh}(\lambda_m (H_1 - Y)) \text{Cos}(\lambda_m Z)}{L \lambda_m \text{Cosh}(\lambda_m H_1)} \\ &- \sum_{n=1}^{\infty} \frac{2 \left(1 + (-1)^{n-1} \right) \gamma_R \bar{\zeta}_s \text{Cosh}(\lambda_n Z) \text{Sin}(\lambda_n Y)}{H_1 \lambda_n \text{Cosh}(\lambda_n L)} \end{aligned} \quad (16)$$

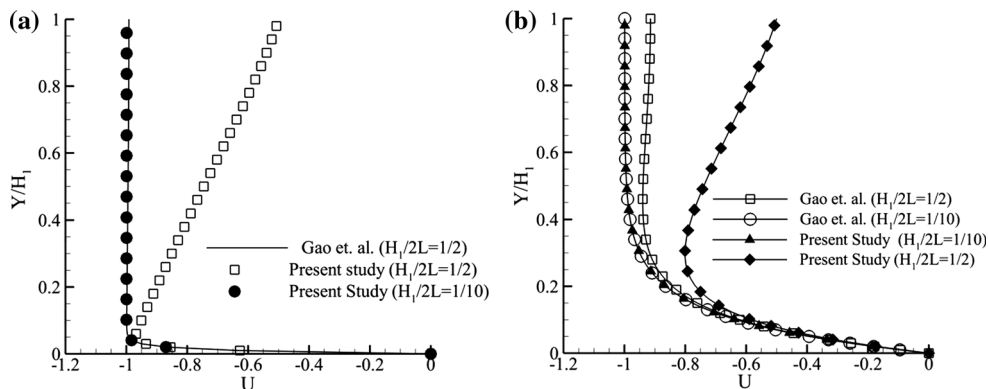
While assuming no-slip and no-penetration at the walls and continuity of stress at the liquid–gas interface for a flat interface, the resulting boundary conditions can be written as,

$$\text{At the walls } (y = 0, z = l) : \vec{u}_1 \cdot \hat{n} = 0, \quad \vec{u}_1 \cdot \hat{t} = 0 \quad (13a)$$

The corresponding flow rate in the rectangular channel can be obtained by,

$$Q_1 = 2 \int_0^L \int_0^{H_1} U_1(Y, Z) dY dZ \quad (17)$$

Fig. 2 Velocity profiles for cases with and without interfacial Maxwell stress at the symmetry axis of the channel ($Z = 0$). The case without Maxwell stress was taken from a study by Gao et al. (2005a, b). The values of fixed parameters are $\gamma_R = 1$, $\zeta_s = 1$, $\zeta_I = 0$, and **a** $De = 0.01$, **b** $De = 0.1$. The free surface is at $Y = H_1$



3 Results and discussions

Using a modified stress term which includes the effects of both hydrodynamic- and electric field-generated stresses, one obtains a body force term in the momentum equations and a modified free surface shear stress jump condition. To observe the effect of Maxwell stress in a free surface electro-osmotic flow, a comparison of velocity profiles with and without modified stress term is presented where the case without interfacial Maxwell stress is taken from Gao et al. (2005a, b) (see Fig. 2). The classical hydrodynamic stress-free condition at the free surface enforces a zero velocity gradient in the direction normal to the free surface. It can be seen that the presence of interfacial Maxwell stress significantly affects the velocity distribution in the fluid. This can result into a dispersive flow which is not observed in a classical EOF. It can also be observed that the effect of Maxwell stress on velocity distribution is greatly enhanced when the channel aspect ratio ($H_1/2L$) is small and the EDL thickness is comparable to the characteristic length scale.

From the velocity solution as obtained in Eq. (16), it can be seen that the fluid velocity distribution is directly proportional to the electro-viscous number, γ_R which represents the ratio of externally applied coulombic forces to the viscous forces. This expected dependence is also evident in classical electro-osmotic flow models where the effect of EDL dynamics is simplified by using a Helmholtz–Smoluchowsky slip velocity ($U_{HS} = -\varepsilon_1 \zeta_b E_{app} / \mu_1$). However, the dependence of fluid velocity on other flow parameters like EDL thickness, wall and interfacial zeta potential and channel geometry is not obvious. The role of each individual parameter on the velocity distribution in the rectangular channel is discussed below.

3.1 Effect of EDL thickness

The thickness of EDL is usually expressed as the Debye length (λ_D) as compared to the flow length scale which in this study is the hydraulic diameter (D_h) represented by the

Debye number (De). The extent of the EDL defines the extent of electrical field-generated body force on the fluid. When the EDL is thin, the charge polarization occurs over a short distance and hence results into very high velocity gradients. This results into large values of the velocity as compared to the case of a thicker EDL where the velocity gradients are smaller. The above observation is evident from Fig. 3 where velocity contours are presented for two different values of the Debye number, namely 0.1 and 0.01 where values of channel aspect ratio, electric field strength, and wall and interfacial zeta potential are fixed.

3.2 Effect of the channel aspect ratio

The channel aspect ratio ($H_1/2L$) determines the effect of channel confinement on the flow characteristics. As compared to the EDL thickness which is determined by the electro-chemistry of the system, the channel geometry is controlled by the limitations of the manufacturing process involved and the physical properties of the material used. From Fig. 4, it is seen that the channel aspect ratio controls the effect of side wall-generated flow on the overall velocity distribution and in some cases on the centerline velocity profile. If the channel aspect ratio is small, the side wall-generated dynamics have a strong effect on the overall velocity profile, whereas if the channel has a larger aspect ratio, the dynamics at the top and bottom boundaries dominate the flow profile. In Fig. 4, the Debye number is taken as 0.1 so that the side wall-generated EOF is more apparent.

3.3 Effect of wall and interfacial zeta potential

The magnitude and polarity of wall and interfacial zeta potential dictate the dominating polarity of charge distribution near the wall or the interface over which the fluid actuating electric field acts. From the Helmholtz–Smoluchowsky relation, one can see that for a positive value of the electric field, the direction of the near wall velocity is opposite to that of the wall zeta potential (see

Fig. 3 Velocity contours in the Y - Z plane for different Debye numbers where $\gamma_R = 1$, $\zeta_s = -1$, $\zeta_I = 1$, $H_1/2L = 1$, and **a** $De = 0.1$, **b** $De = 0.01$. Solid lines show positive velocity and dashed lines show negative velocity values. The free surface is at $Y = H_1$

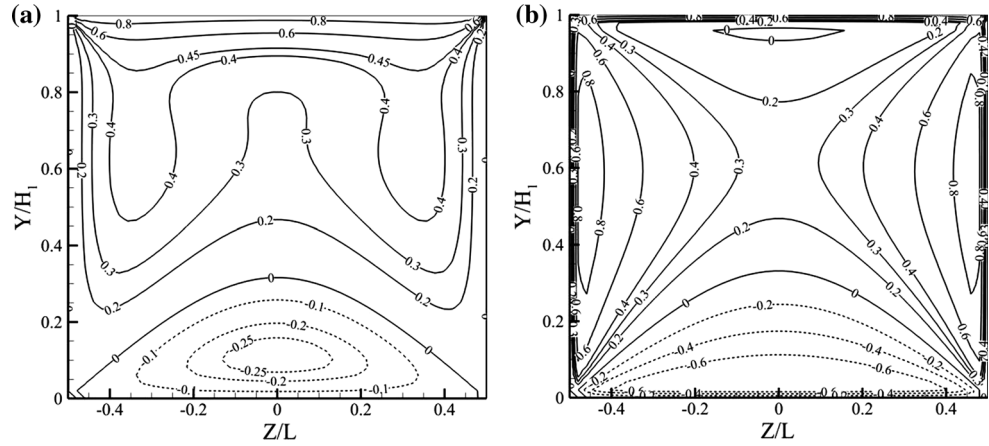
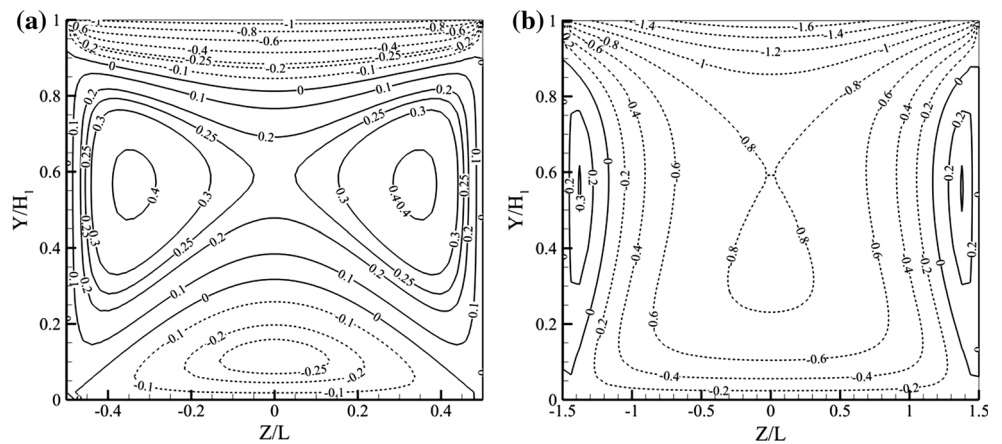


Fig. 4 Velocity contours in the Y - Z plane for different aspect ratios where $De = 0.1$, $\gamma_R = 1$, $\zeta_s = -1$, $\zeta_I = -1$, and **a** $H_1/2L = 1$, **b** $H_1/2L = 1/3$. Solid lines show positive velocity and dashed lines show negative velocity values. The free surface is at $Y = H_1$



Figs. 4a, 5a). However, the direction of the interfacial velocity follows that of the polarity of the interfacial zeta potential. This interesting observation can be attributed to the basic structure of the EDL where the ions contributing to the zeta potential of the substrate are strongly bonded to the surface. For a rigid and stationary substrate, this layer of immobile ions is followed by a layer of mobile oppositely charged ions. For example, if the surface has a negative zeta potential, the mobile ionic layer will be positively charged and under a positive electric field will produce a positive velocity. If the surface is positively charged, the mobile ionic layer will be negatively charged and will produce a negative velocity field under a positive electric field. However, at the interface, there is no rigid and immobile layer of ions and hence the velocity direction is the same as the polarity of the interfacial potential under a positive electric field. This observation is evident in all the velocity field plots. From Fig. 5b, one can see that the polarity of the interfacial potential has a strong influence on the centerline velocity profile and can be controlled to produce desired flow rates in microdevices.

3.4 Flow rate

The net flow rate variation over a range of De manifests various regimes observed in such systems (see Fig. 6). It is remarkable to observe that upon changing the Debye length, which is a function of the salt concentration of the system, one can enhance, diminish, or in some cases, reverse the flow rate in microdevices. The flow reversal observed can be attributed to the combined effects of interfacial zeta potential (ζ_I) and Debye length. It can be seen from Fig. 3 that a positive ζ_I induces a positive interfacial velocity. However, the strength of the extent of this positive velocity in the bulk is delimited by the Debye length, which represents the extent of the polarized cloud of mobile ions. Moreover, for large Debye lengths ($De \geq 0.1$), the positive velocity induced by a positively charged free surface has greater influence over bulk dynamics as compared to the electro-osmotic velocities induced near the walls. This is also evident from Fig. 6a where for a positive ζ_I and sufficiently large Debye length ($De \geq 0.4$), the flow rate is positive irrespective of the polarity of the side walls. It is also observed that the

Fig. 5 **a** Velocity contours on the Y - Z plane where $De = 0.1$, $\gamma_R = 1$, $\zeta_s = 1$, $\zeta_l = -1$, and $H_1/2L = 1/2$. **b** Centerline velocity profile (at $Z = 0$) where $De = 0.1$, $\gamma_R = 1$, $\zeta_s = 1$, and $H_1/2L = 1/2$ for different values of ζ_l

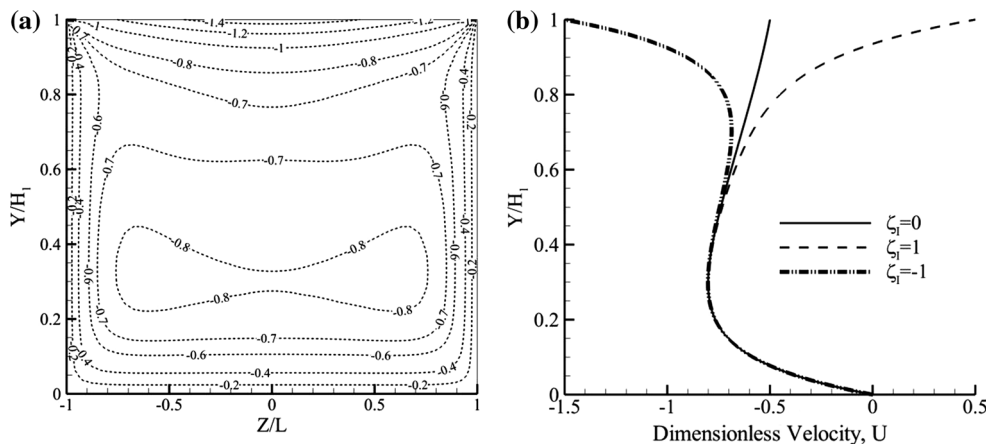
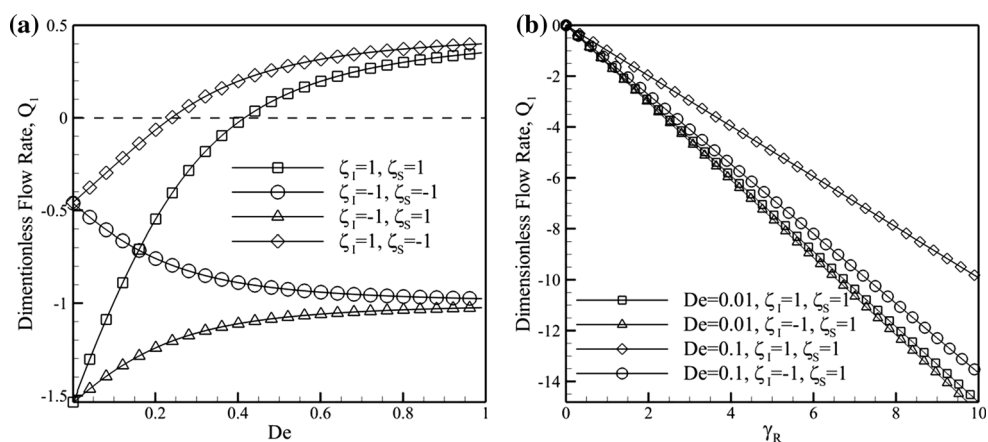


Fig. 6 Dimensionless flow rate variation with **a** Debye number, De for a fixed aspect ratio, $H_1/2L = 1$ and $\gamma_R = 1$. **b** Electro-viscous number, γ_R for a fixed aspect ratio, $H_1/2L = 1$



asymptotic nature of the flow rate dependence helps to identify the regions of maximum and minimum variation of the magnitude of flow rate. This asymptotic variation of flow rate can be attributed to the two prominent opposing mechanisms viz. electro-osmotic actuation and viscous dissipation due to the wall confinements. Such a study helps to control the fluctuations in the electro-osmotically generated flow rates which occur due to the changes in ionic concentrations and pH variations which further culminates into Debye length or zeta potential variations.

From Fig. 6b, it is observed that a reversed polarity of interfacial zeta potential has little effect on the flow rate variation when the Debye layer is thin ($De = 0.01$). However, the reversed polarity of side wall zeta potential changes the flow rate significantly for thin Debye layers (see Fig. 6a). The thin Debye layer case is special as it is the most commonly observed phenomena in experimental microfluidics. Moreover, recent advances allow specific treatment of channel walls to alter their electro-chemical properties, so that one can modulate the substrate zeta

potential to overcome the limitations posed on flow rate by channel geometry through micro-fabrication constraints or the magnitude of the actuating field.

4 Conclusions

The solution of a free surface EOF in a microchannel of rectangular cross section was achieved analytically by taking into account a complete expression of the boundary condition at the free surface that includes the Maxwell stress at this interface. A parametric analysis of the flow in terms of the EDL thickness, channel aspect ratio and different fluid–fluid and solid–fluid interfacial zeta potential was carried out. With the help of two-dimensional velocity contours, it has been shown that the bounding walls have a significant effect on the velocity distribution in a rectangular microchannel. The flow-controlling parameters in an EOF are not only the electro-chemical properties of the involved fluid and electrolytes which control the EDL

thickness and wall and interfacial zeta potentials but also the geometry of the channel through the channel aspect ratio. Moreover, it is observed that by carefully controlling the fluid electro-chemistry for a given geometry of the system and a fixed magnitude of the actuating field, one can enhance or reverse the flow rate. This study also helps to identify the flow control parameters for which the fluctuations in flow rate due to the change in ionic concentration and pH are very low, so that one can achieve the desired flow rate and velocity distribution in a microdevice.

References

- Bhattacharyya S, Zheng Z, Conlisk AT (2005) Electro-osmotic flow in two-dimensional charged micro- and nanochannels. *J Fluid Mech* 540:247
- Bose N, Das T, Chakraborty D, Maiti TK, Chakraborty S (2012) Enhancement of static incubation time in microfluidic cell culture platforms exploiting extended air–liquid interface. *Lab Chip* 12:69–73
- Chang HC, Yossifon G, Demekhin EA (2012) Nanoscale electrokinetics and microvortices: how microhydrodynamics affects nanofluidic ion flux. *Ann Rev Fluid Mech* 44:401–426
- Choi W, Sharma A, Qian S, Lim G, Joo SW (2010) Is free surface free in micro-scale electrokinetic flows? *J Coll Inter Sci* 347:153
- Churaev NV (2000) Liquid and vapor flows in porous bodies: surface phenomena. In: Hughes R (ed) *Topics in chemical engineering*, vol 13. Gordon and Breach, New York
- Gao Y, Wong TN, Yang C (2005a) Transient two-liquid electroosmotic flow with electric charges at the interface. *Coll Surf A* 266:117–128
- Gao Y, Wong TN, Yang C, Ooi KT (2005b) Two-fluid electroosmotic flow in microchannels. *J Coll Inter Sci* 284:306–314
- Griffiths SK, Nilson RH (2006) Charged species transport, separation, and dispersion in nanoscale channels: autogenous electric field-flow fractionation. *Anal Chem* 78:8134–8141
- Lee JSH, Li D (2006) Electroosmotic flow at a liquid–air interface. *Microfluid Nanofluid* 2:361–365
- Levin Y, Dos Santos AP, Diehl A (2009) Ions at the air–water interface: an end to a 100-year-old mystery? *Phys Rev Lett* 103:1–4
- Lin H (2009) Electrokinetic instability in microchannel flows: a review. *Mech Res Commun* 36:33–38
- Marmur A (2004) The lotus effect: superhydrophobicity and metastability. *Langmuir* 20:3517–3519
- Mayur M, Amiroudine S, Lasseux D (2012) Free-surface instability in electro-osmotic flows of ultrathin liquid films. *Phys Rev E* 85:046301
- Ozen O, Aubry N, Papageorgiou DT, Petropoulos PG (2006) Electrohydrodynamic linear stability of two immiscible fluids in channel flow. *Electrochim Acta* 51:5316–5323
- Ramos A (2011) *Electrokinetics and electrohydrodynamics in microsystems*. SpringerWien, New York
- Schoch RB, Han J, Renaud P (2008) Transport phenomena in nanofluidics. *Rev Mod Phys* 80:839–883